2020

Protonation Isomers of Highly Charged Protein Ions Can Be Separated in FAIMS-MS

J. Diana Zhang

Micah T. Donor

Amber D. Rolland

Michael G. Leeming

Huixin Wang

See next page for additional authors

Authors

J. Diana Zhang, Micah T. Donor, Amber D. Rolland, Michael G. Leeming, Huixin Wang, Adam J. Trevitt, K.M. Mohibul Kabir, James S. Prell, and William A. Donald

Protonation isomers of highly charged protein ions can be separated in FAIMS-MS

J. Diana Zhang [a], Micah T. Donor [b], Amber D. Rolland [b], Michael G. Leeming [c], Huixin Wang [d], Adam J. Trevitt [e], K.M. Mohibul Kabir [a], James S. Prell [b], William A. Donald [a, *]

[a] School of Chemistry, University of New South Wales, Sydney, NSW, Australia
[b] Department of Chemistry and Biochemistry and Materials Science Institute, University of Oregon, Eugene, OR, USA
[c] Bio21 Molecular Science and Biotechnology Institute, University of Melbourne, Melbourne, Australia
[d] Solid State & Elemental Analysis Unit, Mark Wainwright Analytical Centre, University of New South Wales, Sydney, NSW, Australia
[e] Molecular Horizons and School of Chemistry and Molecular Bioscience, University of Wollongong, Wollongong, NSW, Australia

A B S T R A C T

High-field asymmetric waveform ion mobility spectrometry-mass spectrometry (FAIMS-MS) can resolve over an order of magnitude more conformers for a given protein ion than alternative methods. Such an expansion in separation space results, in part, from protein ions with masses of >29 kDa undergoing dipole alignment in the high electric field of FAIMS, and the resolution of ions that adopt pendular vs free rotor states. In this study, FAIMS-MS, collision-induced dissociation (CID), and travelling wave (TW) IMS-MS were used to investigate the pendular and free rotor states of protonated carbonic anhydrase II (CAII, 29 kDa). The electrospray ionization additive 1,2-butylene carbonate was used to increase protein charge states and ensure extended ion conformations were formed. For relatively high charge states in which dipole alignment occurs (30−38+), FAIMS-MS can baseline resolve the isobaric pendular and free rotor ion populations. For TWIMS-MS, these same charge states resulted in monomodal arrival time distributions with collision cross sections corresponding to highly extended ion conformations. Interestingly, CID of FAIMS-selected pendular and free rotor ion populations resulted in significantly different fragmentation patterns. For example, CID of the dipole aligned CAII 37+ resulted in cleavages C-terminal to residue 183, 192 and 196, whereas cleavage sites for the free rotor population occurred near residues 12 and 238. Given that the cleavage sites are 'directed' by protonation sites in the CID of protein ions, and highly charged protein ions adopt extended conformations with the same or very similar collision cross sections, these results indicate that the pendular and free rotor populations separated in FAIMS can be attributed to protonation isomers. Moreover, the extent of protein ion charging in FAIMS-MS decreased substantially as the carrier gas flow rate decreased, indicating that ion charging in FAIMS-MS can be limited by proton-transfer reactions. Given that the total mass of proton charge carriers corresponds to less than 0.2% the mass of CAII, we anticipate that FAIMS-MS can be used to separate intact isobaric proteoforms with masses of at least ~29 kDa that result from alternative sites of post-translational modifications.

1. Introduction

Ion mobility spectrometry (IMS) is well-known for its ability to rapidly separate many different types of ions nearly simultaneously for sensitive detection by mass spectrometry (MS) [1,2]. The most common IMS methods separate ions along the direction of travel as they traverse a linear distance through a buffer gas under the influence of a relatively low DC or pulsed electric field (E), such as in

Dedicated to the memory of Professor Michael Guilhaus (UNSW Sydney) who was the second recipient of Curt Brunnée Award (1997) from the International Mass Spectrometry Foundation.

drift tube IMS or travelling wave (TW) IMS, respectively [3]. Typically, such separated ions are detected within microseconds with high sensitivity using an orthogonal acceleration time-of-flight mass analyser that was re-invented and developed in the mid-to-late 1980s [4–8] for which Professor Michael Guilhaus received the 1997 Curt Brunnée Award. Under low E/N (N is the gas number density), ion drift velocity increases linearly with electric field and is strongly dependent on the ion's collision cross-section, mass and charge state. High-field asymmetric waveform ion mobility spectrometry (FAIMS) enables ion separations to be performed using extremely high electric fields such that mobility depends non-linearly on E/N. Additional to high-field ion transport phenomena, such as ion-neutral declustering, field heating, inelastic collisions, and Non-Blanc phenomena [9], can also occur in FAIMS. Moreover, the ion separations in FAIMS typically occur at atmospheric pressure, which can be beneficial in innovative portable ion 'sensing' and tandem FAIMS-FAIMS applications without constraints associated with vacuum systems [10,11].

In FAIMS, ions are carried by a gas between two parallel electrodes. An asymmetric waveform of a given amplitude (or dispersion voltage, DV) is applied between the electrodes separated by a distance d resulting in a maximum electric field, E_D (DV/d). By use of the asymmetric field, ions are separated laterally to the direction of flow based on their differential mobility in the high and low electric fields. In FAIMS, ions can be classified into at least three types: (i) ion mobility increases with increasing electric field (A-type); (ii) ion mobility decreases with increasing electric field (C-type); and (iii) ion mobility increases and then decreases with increasing electric field (B-type) [9]. The type of ion behaviour in FAIMS can depend strongly on ion solvation effects, in which greater ion-solvent clustering can result in enhanced A- or B-type behaviour [12]. To compensate for the change in ion mobility, a compensation voltage (CV) or compensation field E_C (CV/d) is superimposed on the waveform and can be tuned to selectively correct the ion's lateral displacement. For example, a positive E_C is applied to transmit C-type ions and a negative E_C is applied to transmit A-type ions. By scanning the CV, a spectrum of ions can be obtained. Since FAIMS separates ions based on differential mobilities, ion separations can be substantially more orthogonal to m/z than for low field separations [13], and can enable the separation of many different types of *isobaric* ions, including 'middle-down' proteoforms [14,15], peptides with alternative sites of chemical modifications [16–19], isomeric perfluoroalkyl substances [20], diastereomers [21–23], and small molecules [24,25].

FAIMS-MS is particularly promising for the analysis of whole proteins. For example, FAIMS can separate >10 intact protein conformers – at moderate-to-high charge states – of ubiquitin, cytochrome *c* and myglobin [26,27]. For larger proteins, FAIMS can separate over a magnitude more protein ion conformations than most IMS methods [1]. One of the reasons for this enhanced separation capability for FAIMS is the phenomenon of dipole alignment [1,28]. For proteins such as carbonic anhydrase (~29 kDa), transferrin (~78 kDa) and serum albumin (~66 kDa), ions can undergo a reversible dipole alignment under high electric field, in which the dipole moment for these protein ions exceeds the 450 D threshold required for dipole alignment to occur under typical FAIMS conditions (atmospheric pressure and ambient temperature) [1,28]. That is, ions > 30 kDa will shift from C-type to A-type (or B-type) behaviour. As a consequence of dipole alignment, the directional cross section is smaller than the rotationally averaged cross section and thus, ion mobility will increase resulting in A-type (or B-type) ion behaviour [29]. That is, A- or B-type correspond to pendular or aligned ion states and C-type to free rotor or unaligned states for proteins ~29 kDa and higher in mass. Given the enhanced ability to separate a relatively large number of protein conformations, the separation of isobaric intact proteins that differ by alternative sites of post translational modifications using FAIMS is becoming feasible.

Herein, we investigated the origins of the pendular and free rotor states of a ~29 kDa protein (carbonic anhydrase II) that is of an 'ideal' size to adopt both pendular and free-rotor states during FAIMS-MS separations. Because different 3D conformations of a protein ion should have different dipole moments, we used a chemical supercharger 1,2-butylene carbonate (BC) as an ESI additive to increase the charge states of protonated carbonic anhydrase and ensure that protein ions adopt extended conformations. Given that FAIMS resolution is proportional to $z^{1/2}$ (z = charge state) [26], protein ion supercharging should 'in principle' improve ion separation in FAIMS. Based on FAIMS-MS, CID and TWIMS-MS measurements, we report that the pendular and free rotor states of highly charged carbonic anhydrase II (CAII, ~29 kDa) can correspond to protonation isomers that are in extended protein ion conformations and have nearly the same collision cross sections. Moreover, the extent of protein ion charging in FAIMS-MS can be limited by proton-transfer reactions at atmospheric pressure.

2. Method

2.1. Materials

Carbonic anhydrase II from bovine erythrocytes was obtained from Sigma Aldrich and used without further purification. BC was obtained from Tokyo Chemical Industry. Deionized ultrapure water (18 MΩ cm) was obtained using a water purification system (MilliQ, Merck). Methanol and acetic acid were obtained from Merck and Chem Supply, respectively. Stock solutions of carbonic anhydrase II were prepared in deionized water. For FAIMS-MS experiments, sample solutions of CAII (20 μM) were prepared in 99:1 methanol: acetic acid; supercharged solutions were prepared in 94:5:1 methanol:BC:acetic acid. For TWIMS-MS experiments, sample solutions of CAII were prepared in 94:5:1 methanol:BC:acetic acid.

2.2. Instrumentation and calculations

All FAIMS-MS experiments were carried out on a modified linear quadrupole ion trap MS (LTQ XL, Thermo Scientific, San Jose, CA, USA) that is equipped with a custom ion funnel, a high-resolution FAIMS device (Heartland Mobility, KS, USA), and an ESI source. For ESI, sample solutions were infused at 1 μL/min into a borosilicate capillary emitter (76 μm inner diameter), and a voltage of +3.5 kV was applied to the solution relative to the curtain plate entrance of the FAIMS device. For FAIMS-MS, an E_D of 22 kV/cm was applied and a N_2(g) carrier gas with a flow rate of 2–4 L/min was used. Flowrates of less than 2 L/min resulted in very low signal-to-noise under these conditions and were not used subsequently. Full details of the FAIMS-MS experiments are detailed elsewhere [21,22]. Collision-induced dissociation (CID) of ions that were selected by FAIMS-MS was performed using normalised collision energy of 2% and an isolation window of 4 m/z centred on the ion of interest (Table S1). To confirm sequence ion assignments, the CID mass spectra were also measured using a hybrid linear quadrupole ion trap-orbitrap MS (LTQ Orbitrap XL, Thermo Scientific, San Jose, CA, USA) [30]. Sequence ions were processed using MASH-Suite [31]. For TWIMS-MS experiments, a Synapt G2-Si (Waters) equipped with a nanoelectrospray ionization source was used as described previously [32]. CCS values were obtained from ion arrival time distributions by an established calibration method [33]. Both extended-chain and α-helical structures of CAII were constructed in Avogadro [34], and the corresponding CCS values were computed using Collidoscope in a method described previously

[32,35]. Details of the TWIMS-MS experiments (Table S2), experimental drift time values, and the CCS calibration methodology can be found in the Supplementary Information. Predicted protonation sites were calculated using PredictPrPlus [30,36], which was modified to export detailed protonation configurations within specified energy thresholds (refer to Table S3 for input parameters).

3. Results and discussion

3.1. Effects of FAIMS-MS on protein ion charging

Solution additives such as BC can be used to significantly increase protein ion charging in ESI-MS [37–41]. The mass spectra of solutions containing CAII, with or without 5% v/v BC, are shown in Fig. 1. In ESI-MS, the addition of BC increased the average (abundance weighted) charge state from 34.0 ± 0.1 to 44.3 ± 0.4, which is comparable to previous reports [37,38]. In contrast, by using ESI-FAIMS-MS (without separation, i.e. no asymmetric waveform applied), the addition of BC at a carrier gas flow rate of 2 L/min N_2 had minimal effect. For example, the average charge state was 32.5 ± 0.1 without using BC compared to 31.31 ± 0.01 using BC. However, the average charge state of CAII increased steadily and monotonically from 31.31 ± 0.01 to 40.6 ± 0.1 as the gas flow rate increased from 2 L/min to 4 L/min (Supplementary Fig. 1). The higher flow rate of 4 L/min corresponds to an ion residence time in the FAIMS device of 0.1 s as opposed to 0.2 s for 2 L/min. Since higher charge states are formed when ions spend less time in the FAIMS device, these data suggest that protein charge stripping can occur with lower flow rates and correspondingly longer ion residence times. Highly charged protein ions in which approximately every fourth residue is protonated on average (CAII ~40+ and higher) can readily transfer a proton to N_2 at reduced pressure when stored in a linear quadrupole ion trap (<1 mTorr of N_2) [36,42]. Given that the partial pressure of N_2 in ambient pressure FAIMS experiments is five orders of magnitude higher (~760 Torr) [36,] than in the previous ion-trap proton-experiments (<1 mTorr) [36], the 40+ and higher charge states of CAII are expected to readily transfer protons to N_2(g) during transit between the FAIMS electrodes. Any impurities more basic than N_2 in the carrier gas may also contribute to reducing protein ion charging by proton transfer reactions. Because the resolving power in FAIMS decreases with shorter ion residence times [43], any improvement to resolution in FAIMS by the formation of CAII in higher charged states is limited by proton transfer reactions with ambient gases under these conditions.

3.2. Comparison between TWIMS and FAIMS-MS

Representative FAIMS-MS spectra and TWIMS-MS arrival time distributions for CAII 26+ to 38+ are shown in Supplementary Fig. 2. For charge states higher than 30+, FAIMS-MS resulted in two baseline separated peaks (E_C ~ −179 to −154 V/cm and +23 to +24 V/cm), whereas lower charge states resulted in a single peak (E_C ~ +25 to +36 V/cm). These data are consistent with at least one sub-population of ions in FAIMS-MS that can undergo dipole alignment (charge states 30+ to 38+ with A- or B-type behaviour) and another population that does not (charge states 26+ to 38+ with C-type behaviour). That is, pendular states are observed for charge states 30+ to 38+, and free rotor states for charge states 26+ to 38+, consistent with previous reports [28]. For charge states higher than 30+, the E_C of the A-type population shifts to more negative values from ~ −156 V/cm (31+) to ~ −178 V/cm (38+) as the charge state increases (Fig. S2), which can be attributed to enhanced ion-neutral clustering during the low field portion of the FAIMS waveform as charge state increases. This result is consistent with more highly charged ions having higher sequential ion-neutral binding energies than those with fewer charges [44–46]. In addition, the peak abundances of the C-type ions decreased as charge state increased from 26+ to ~34+ and the abundances of this ion type increased at higher charge states. While the origin for

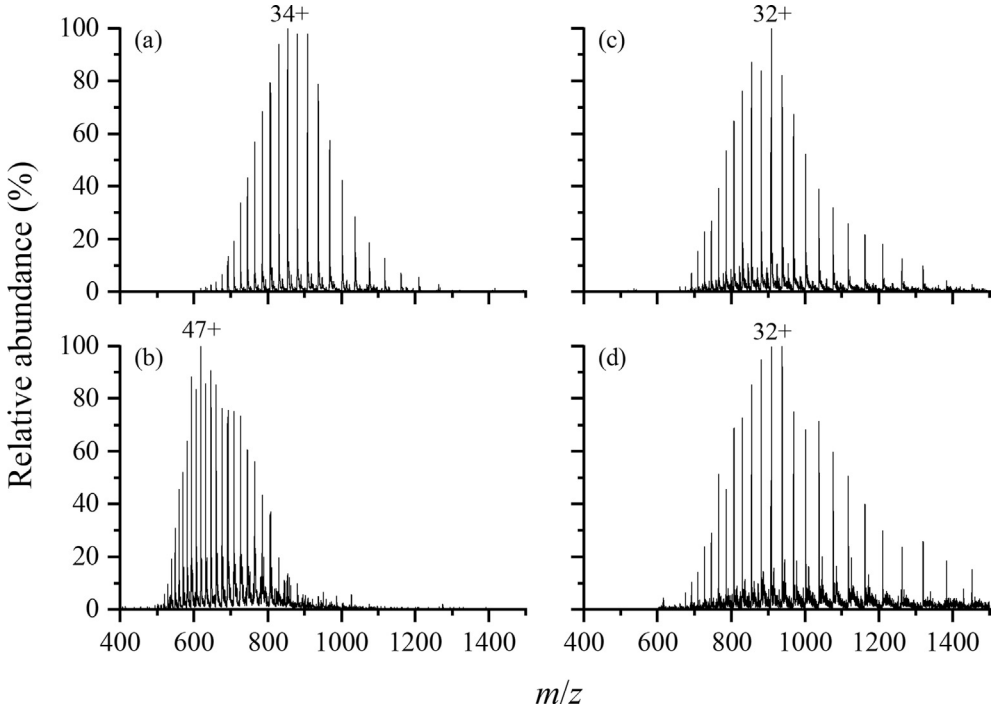

Fig. 1. The extent of protein ion 'supercharging' can be limited by using FAIMS-MS. Comparison of ESI mass spectra of CAII with either (a) no BC, or (b) 5% v/v BC; and ESI-FAIMS mass spectra of CAII (without using an asymmetric waveform for ion separation) at a gas flow rate of 2 L/min N_2 either with (c) no BC, or (b) 5% v/v BC.

this phenomenon is unclear, one possible explanation can be attributed to the differences in the total number of energetically low-lying proton configurations (see below).

In contrast, TWIMS-MS for the same charge states resulted in single arrival time peaks for each charge state (Supplementary Fig. 2). The corresponding CCS values for CAII 26+ to 38+ are shown in Supplementary Table 4 and Supplementary Fig. 3. Both extended-chain and α-helical structures were also calculated for the three charge states (Supplementary Fig. 3). The experimental CCS values increased from 75.1 to 85.6 nm^2 for charge states 26+ to 38+, respectively, which were between the calculated rotationally averaged CCS values for extended-chain (~102 nm^2) and α-helical structures (~62 nm^2). Given that CCS increases as a function of charge state and are between the predicted CCS values for extended-chain and α-helical structures, these results indicate that the ion population may include both 'extended' and α-helical motifs, and that more elongated conformers are found for charge states >30+ (CCS > 79 Å). Previous studies have demonstrated that the charge states of protein ions formed from native solutions that are separated by FAIMS can have substantially different gas-phase hydrogen-deuterium exchange kinetics [47] and electron capture cross sections [48], consistent with FAIMS-separated isobaric charge states having significant conformational differences. However, such observations have not been reported for FAIMS-separated isobaric protein ions in high charge states with elongated conformations.

3.3. Collision-induced dissociation of FAIMS-selected intact protein ions

Collision-induced dissociation data of FAIMS-selected intact protein ions for three different charge states of CAII (27+, 32+, and 37+) were obtained for the pendular states (32+ and 37+) and free rotor states (27+, 32+, and 37+) (Fig. 2). These charge states are representative of ions in relatively low to high charge states that have pendular states and/or free rotor states in FAIMS-MS separations. For both the 32+ and 37+ charge states, CID of free rotor and pendular states transmitted at either positive or negative E_C, respectively, resulted in different fragmentation spectra. Specifically, the 32+ charge state fragmented to yield unique cleavage sites at negative E_C (C-terminal to Leu_{196} and Thr_{198}). Similarly, the 37+ charge state yielded unique cleavage sites at negative E_C (C-terminal to Leu_{183}, Tyr_{192}, and Leu_{196}) and positive E_C (N-terminal to Pro_{12} and C-terminal to Leu_{238}). Because cleavage sites in intact protein ions are 'driven' by the location of protons before and during ion activation [30,49], the difference in the measured cleavage sites for pendular and free rotor states indicates that the proton locations are different in these two ion populations. In the absence of FAIMS separation, CID of CAII 32+ and 37+ correspond to a linear superposition of the fragmentation patterns of FAIMS separated pendular and free rotor states as expected. For example, the summed abundances for the free rotor states (relative population of ~37%) and pendular states (~63%) at each cleavage site for 37+ are within an average of ~35% of those resulting from CID of the unseparated 37+.

3.4. Calculated proton configurations

Predicted proton configurations for the 27+, 32+, and 37+ charge states were also calculated using a simple electrostatic model implemented in PredictPrPlus [30,36] which was modified slightly to store all proton configurations within a specified energy relative to the ground state configuration (Supplementary Fig. 4, and Supplementary Tables 5–7). In this approach, the extended protein ions are modelled as 1D line segments with each amino acid residue corresponding to a node with a given intrinsic gas-phase basicity, and electrostatic repulsion is accounted for using Coulomb's law [30,36]. A given number of protons are randomly distributed along the protein backbone and the energy is minimised by semi-randomly moving each proton to a different node and calculating the configuration energy. The protons are then randomly distributed again, and re-optimised. The lowest energy configurations within a given energy were then stored after 30,000 computational iterations.

For the 27+, 32+, and 37+ charge states, a total of 172, 6, and 18 different proton configurations were calculated to be within 12 kJ/mol of the lowest energy configuration. Most protons were located at basic amino acid residues (i.e. Arg, Lys, His, and the N-terminus). However, 3, 6, and 11 protons for charge states 27+, 32+, and 37+, respectively, were located at low basicity residues (i.e. not Arg, Lys, His or the N-terminus). Specifically, 2, 3, and 4 protons for charge states 27+, 32+, and 37+, respectively, were located near residues 175 to 200 where no basic residues are present. Previous research has demonstrated that in the CID of highly charged protein ions, cleavage sites occur near the first low basicity residues that are predicted to be protonated with increasing charge state [30]. For the CID of the pendular and free rotor separated protein ions, cleavage sites also occurred near the predicted sites of protons at low basicity residues. For example, CID of the 32+ ion resulted in cleavage sites C-terminal to residues Trp-190 and Pro-199, which are near predicted sites of protonation (Fig. 2). Furthermore, the protons that are calculated to be in different locations from the lowest energy configuration for higher energy configurations are shown in Supplementary Fig. 4. For all three charge states, the protons that are in different locations in higher energy configurations tend to be located near low basicity residues in the lowest energy calculated configuration, and these protons are clustered near the C-terminal side of the protein, particularly for the 27+ and 32+, which is also where most of the differences in cleavage sites occur for the pendular and free rotor separated protein ions. Given that the predicted protonation sites correspond well with the measured cleavage sites in CID and that the CCS of each ion population are very similar, these data suggest that free rotor and pendular states, which can be separated by FAIMS-MS, correspond primarily to protonation isomers that have very similar or the same (rotationally averaged)collision cross sections. Differences in proton configurations and low-field ion-neutral clustering that occur in FAIMS should impact the dipole moments of ion species and thus enable protomer separation. Considering that many energetically low-lying proton configurations are possible, these results also suggest that FAIMS can separate two sub-populations of many different protonation isomers, or ensembles of protomers. The extent and location of alpha helical motifs, or other structural features, within elongated protein ion conformations may yield ions of a given charge state with similar CCS (that cannot be resolved by TWIMS-MS) and may also contribute to the separation of protonation isomers in FAIMS-MS.

4. Conclusion

Dipole alignment in FAIMS contributes to a unique phenomenon in which protein ions with masses > ~29 kDa can exhibit both pendular and free rotor states, which can be separated and significantly enhance the separation space for intact protein ions. FAIMS of protonated carbonic anhydrase II ions (30–38+) results in two baseline separated ion populations for each charge state corresponding to free rotor and pendular states, whereas TWIMS results in a single arrival time distribution for each charge state. Based on the TWIMS measurements, the highly charged CAII ions (30–38+) adopt elongated conformations. Collision-induced dissociation of

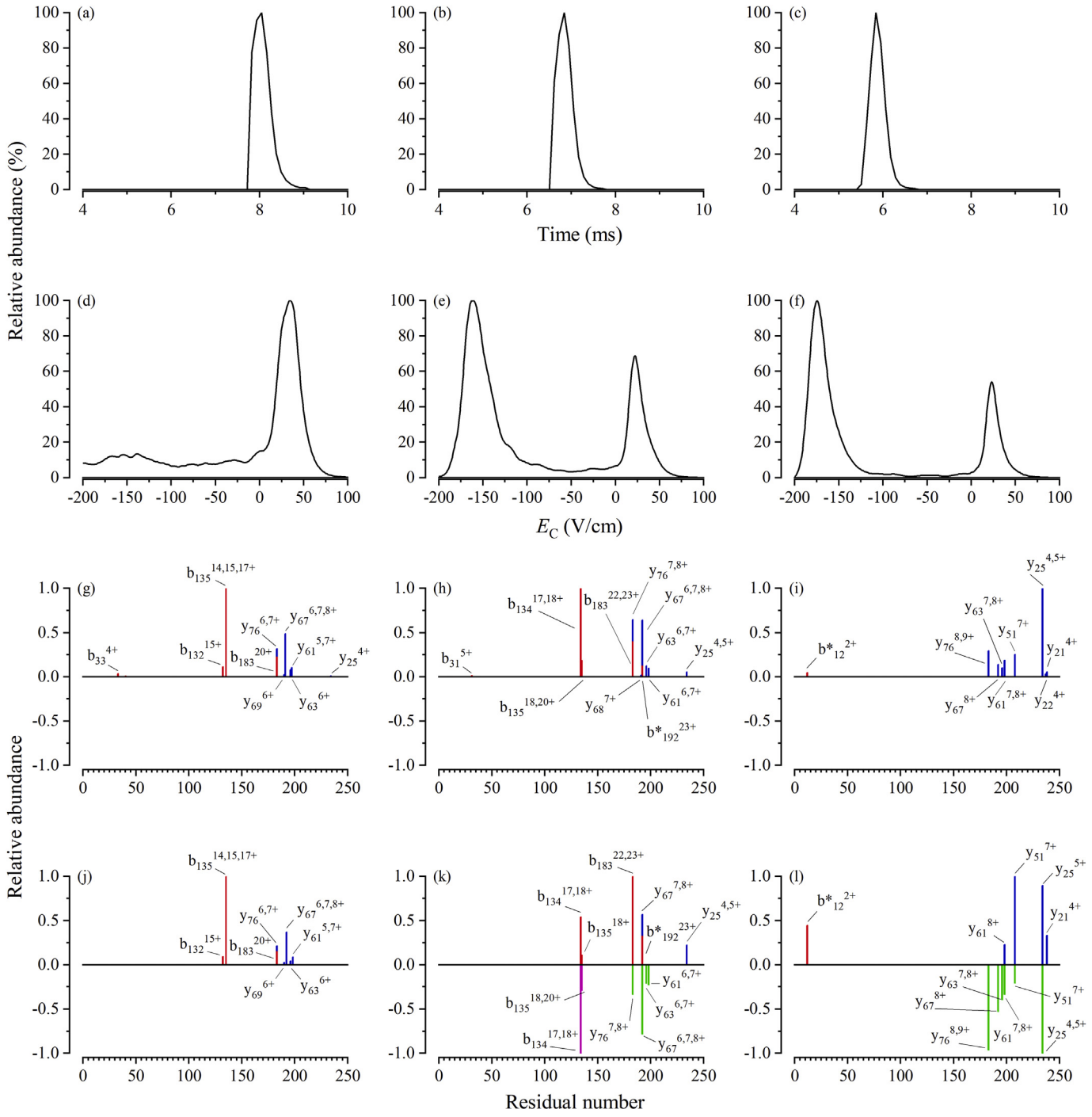

Fig. 2. Isobaric protonation isomers can be resolved in FAIMS-MS. Charge states 27+ (a, d, g, j), 32+ (b, e, h, k), and 37+ (c, f, i, l) from: TWIMS-MS arrival time distribution (a–c); FAIMS-MS distribution (d–f); CID-FAIMS-MS without separation (g–i); CID-FAIMS-MS with separation (j–l). Positive abundance indicates CID taken from free rotor states (C-type) at positive E_C; negative abundance indicates CID taken pendular states (A- or B-type) at negative E_C. Red/pink = b sequence ions; blue/green = y sequence ions. b* indicates (b − NH_3) sequence ions. (For interpretation of the references to colour in this figure legend, the reader is referred to the Web version of this article.)

FAIMS-selected free rotor and pendular states of protonated CAII ions (32+ and 37+) resulted in substantially different fragment ion spectra, and the formation of unique sequences ions primarily clustered near the C-terminal half of the protein. Cleavage sites tended to occur near predicted protonation sites at low basicity amino acid residues, consistent with cleavages being driven by protonation sites both prior to and/or during ion activation in CID [30,49]. These results indicate that FAIMS-MS can resolve protomer ensembles of the same mass, charge, and essentially the same rotationally-averaged (i.e. low-field) collision cross sections, but different dipole moments. The extent of protein ion charging increases strongly as the carrier gas flow rate increases and corresponding ion residence time decreases, which indicates that protein ion charging is limited by proton transfer reactions in FAIMS-MS under these conditions. Given that CID can result in the migration of protonation sites during ion activation, the integration

of FAIMS with complementary ion activation methods that can cleave backbone protein ions bonds with minimal 'scrambling' of labile hydrogen atoms or protons, such as ultraviolet photodissociation, should be particularly useful for assigning charge site locations and probing conformational folding and/or refolding of pendular and free rotor states after ion separation [50–52]. It is anticipated that by performing FAIMS at reduced pressures [53,54], protein ion supercharging can be used to increase the performance of denatured protein ion separations. Given that isobaric 'protomers' of an intact 29 kDa protein ion can be separated, we anticipate that FAIMS will be beneficial in the analysis of intact proteoforms that differ by alternative sites of post-translational modifications, such as phosphorylations, which can significantly impact charge configurations of whole protein ions.

CRediT authorship contribution statement

J. Diana Zhang: Writing - original draft, Methodology, Formal analysis, Investigation. **Micah T. Donor:** Methodology, Formal analysis, Investigation. **Amber D. Rolland:** Methodology, Formal analysis, Investigation. **Michael G. Leeming:** Methodology. **Huixin Wang:** Methodology. **Adam J. Trevitt:** Funding acquisition, Conceptualization, Validation. **K.M. Mohibul Kabir:** Funding acquisition, Validation. **James S. Prell:** Supervision, Validation. **William A. Donald:** Writing - review & editing, Supervision, Funding acquisition, Conceptualization, Validation, Formal analysis, Investigation.

Declaration of competing interest

The authors declare that they have no known competing financial interests or personal relationships that could have appeared to influence the work reported in this paper.

Acknowledgements

AJT and WAD acknowledge support from the Australian Research Council (DP200100065). KMMK acknowledges support from the Australian Research Council (DE190100986). We thank the Bioanalytical Mass Spectrometry Facility at UNSW Sydney for access to some instrumentation.

Appendix A. Supplementary data

Supplementary data to this article can be found online at https://doi.org/10.1016/j.ijms.2020.116425.

References

[1] A.A. Shvartsburg, S.Y. Noskov, R.W. Purves, R.D. Smith, Pendular proteins in gases and new avenues for characterization of macromolecules by ion mobility spectrometry, Proc. Natl. Acad. Sci. U.S.A. 106 (16) (2009) 6495–6500.
[2] V. Gabelica, A.A. Shvartsburg, C. Afonso, P. Barran, J.L.P. Benesch, C. Bleiholder, M.T. Bowers, A. Bilbao, M.F. Bush, J.L. Campbell, I.D.G. Campuzano, T. Causon, B.H. Clowers, C.S. Creaser, E. De Pauw, J. Far, F. Fernandez-Lima, J.C. Fjeldsted, K. Giles, M. Groessl, C.J. Hogan Jr., S. Hann, H.I. Kim, R.T. Kurulugama, J.C. May, J.A. McLean, K. Pagel, K. Richardson, M.E. Ridgeway, F. Rosu, F. Sobott, K. Thalassinos, S.J. Valentine, T. Wyttenbach, Recommendations for reporting ion mobility Mass Spectrometry measurements, Mass Spectrom. Rev. 38 (3) (2019) 291–320.
[3] R. Cumeras, F. E, C.E. Davis, J.I. Baumbach, I. Gracia, Review on ion mobility spectrometry. Part 1: current instrumentation, Analyst 140 (2015) 1376–1390.
[4] A. Sosimenko, Thesis, University of New South Wales, Sydney, 1987.
[5] J.H.J. Dawson, M. Guilhaus, US PCT No. PCT/AU88/00498 Filed, 23 Dec, 1988. Published June 29, 1989 Foreign Application Priority Australian Provisional Patent PCT 16079. December 24, 1987.
[6] J.H.J. Dawson, M. Guilhaus, Orthogonal-acceleration time-of-flight mass spectrometer, Rapid Commun. Mass Spectrom. 3 (5) (1989) 155–159.
[7] J. Coles, M. Guilhaus, Orthogonal acceleration — a new direction for time-of-flight mass spectrometry: fast, sensitive mass analysis for continuous ion sources, TrAC Trends Anal. Chem. (Reference Ed.) 12 (5) (1993) 203–213.
[8] M.M. Sheil, Critical moments in time: reflections on the development of orthogonal acceleration time-of-flight mass spectrometry, J. Am. Soc. Mass Spectrom. 23 (8) (2012) 1301–1305.
[9] A.A. Shvartsburg, Differential Ion Mobility Spectrometry: Nonlinear Ion Transport and Fundamentals of FAIMS, CRC Press, Florida, 2008.
[10] G.A. Eiceman, E.V. Krylov, N.S. Krylova, E.G. Nazarov, R.A. Miller, Separation of ions from explosives in differential mobility spectrometry by vapor-modified drift gas, Anal. Chem. 76 (17) (2004) 4937–4944.
[11] G.A. Eiceman, E.G. Nazarov, R.A. Miller, E.V. Krylov, A.M. Zapata, Micromachined planar field asymmetric ion mobility spectrometer as a gas chromatographic detector, Analyst 127 (4) (2002) 466–471.
[12] C. Liu, J.C.Y. Le Blanc, J. Shields, J.S. Janiszewski, C. Ieritano, G.F. Ye, G.F. Hawes, W.S. Hopkins, J.L. Campbell, Using differential mobility spectrometry to measure ion solvation: an examination of the roles of solvents and ionic structures in separating quinoline-based drugs, Analyst 140 (20) (2015) 6897–6903.
[13] K.M.M. Kabir, W.A. Donald, Microscale differential ion mobility spectrometry for field deployable chemical analysis, TrAC Trends Anal. Chem. (Reference Ed.) 97 (2017) 399–427.
[14] A. Garabedian, M.A. Baird, J. Porter, K. Jeanne Dit Fouque, P.V. Shliaha, O.N. Jensen, T.D. Williams, F. Fernandez-Lima, A.A. Shvartsburg, Linear and differential ion mobility separations of middle-down proteoforms, Anal. Chem. 90 (4) (2018) 2918–2925.
[15] P.V. Shliaha, V. Gorshkov, S.I. Kovalchuk, V. Schwämmle, M.A. Baird, A.A. Shvartsburg, O.N. Jensen, Middle-down proteomic analyses with ion mobility separations of endogenous isomeric proteoforms, Anal. Chem. 92 (3) (2020) 2364–2368.
[16] D.L. Winter, J. Mastellone, K.M.M. Kabir, M.R. Wilkins, W.A. Donald, Separation of isobaric mono- and dimethylated RGG-repeat peptides by differential ion mobility-mass spectrometry, Anal. Chem. 91 (18) (2019) 11827–11833.
[17] M.A. Baird, A.A. Shvartsburg, Localization of post-translational modifications in peptide mixtures via high-resolution differential ion mobility separations followed by electron transfer dissociation, J. Am. Soc. Mass Spectrom. 27 (12) (2016) 2064–2070.
[18] J.L. Kaszycki, A.P. Bowman, A.A. Shvartsburg, Ion mobility separation of peptide isotopomers, J. Am. Soc. Mass Spectrom. 27 (5) (2016) 795–799.
[19] K. Jeanne Dit Fouque, A. Garabedian, J. Porter, M. Baird, X. Pang, T.D. Williams, L. Li, A. Shvartsburg, F. Fernandez-Lima, Fast and effective ion mobility–mass spectrometry separation of d-amino-acid-containing peptides, Anal. Chem. 89 (21) (2017) 11787–11794.
[20] E. Ahmed, K.M. Mohibul Kabir, H. Wang, D. Xiao, J. Fletcher, W.A. Donald, Rapid separation of isomeric perfluoroalkyl substances by high-resolution differential ion mobility mass spectrometry, Anal. Chim. Acta 1058 (2019) 127–135.
[21] J.D. Zhang, K.M.M. Kabir, W.A. Donald, Metal-ion free chiral analysis of amino acids as small as proline using high-definition differential ion mobility mass spectrometry, Anal. Chim. Acta 1036 (2018) 172–178.
[22] J.D. Zhang, K.M.M. Kabir, H.E. Lee, W.A. Donald, Chiral recognition of amino acid enantiomers using high-definition differential ion mobility mass spectrometry, Int. J. Mass Spectrom. 428 (2018) 1–7.
[23] J.D. Zhang, K.M. Mohibul Kabir, W.A. Donald, Chapter three - ion-mobility mass spectrometry for chiral analysis of small molecules, in: W.A. Donald, J.S. Prell (Eds.), Comprehensive Analytical Chemistry, vol. 83, Elsevier, 2019, pp. 51–81.
[24] S.J.P. Marlton, B.I. McKinnon, B. Ucur, A.T. Maccarone, W.A. Donald, S.J. Blanksby, A.J. Trevitt, Selecting and identifying gas-phase protonation isomers of nicotineH+ using combined laser, ion mobility and mass spectrometry techniques, Faraday Discuss 217 (2019) 453–475, 0.
[25] S.J.P. Marlton, B.I. McKinnon, B. Ucur, J.P. Bezzina, S.J. Blanksby, A.J. Trevitt, Discrimination between protonation isomers of quinazoline by ion mobility and UV-photodissociation action spectroscopy, J. Phys. Chem. Lett. 11 (10) (2020) 4226–4231.
[26] A.A. Shvartsburg, R.D. Smith, Separation of protein conformers by differential ion mobility in hydrogen-rich gases, Anal. Chem. 85 (14) (2013) 6967–6973.
[27] A.A. Shvartsburg, Ultrahigh-resolution differential ion mobility separations of conformers for proteins above 10 kDa: onset of dipole alignment? Anal. Chem. 86 (21) (2014) 10608–10615.
[28] A.A. Shvartsburg, T. Bryskiewicz, R.W. Purves, K. Tang, R. Guevremont, R.D. Smith, Field asymmetric waveform ion mobility spectrometry studies of Proteins: dipole alignment in ion mobility spectrometry? J. Phys. Chem. B 110 (43) (2006) 21966–21980.
[29] H.J. Cooper, To what extent is FAIMS beneficial in the analysis of proteins? J. Am. Soc. Mass Spectrom. 27 (4) (2016) 566–577.
[30] H. Wang, M.G. Leeming, J. Ho, W.A. Donald, Origin and prediction of highly specific bond cleavage sites in the thermal activation of intact protein ions, Chem. Eur J. 25 (3) (2019) 823–834.
[31] H. Guner, P.L. Close, W. Cai, H. Zhang, Y. Peng, Z.R. Gregorich, Y. Ge, MASH suite: a user-friendly and versatile software interface for high-resolution mass spectrometry data interpretation and visualization, J. Am. Soc. Mass Spectrom. 25 (3) (2014) 464–470.
[32] S.A. Ewing, M.T. Donor, J.W. Wilson, J.S. Prell, Collidoscope: an improved tool for computing collisional cross-sections with the trajectory method, J. Am.

Soc. Mass Spectrom. 28 (4) (2017) 587–596.
[33] B.T. Ruotolo, J.L.P. Benesch, A.M. Sandercock, S.-J. Hyung, C.V. Robinson, Ion mobility–mass spectrometry analysis of large protein complexes, Nat. Protoc. 3 (7) (2008) 1139–1152.
[34] M.D. Hanwell, D.E. Curtis, D.C. Lonie, T. Vandermeersch, E. Zurek, G.R. Hutchison, Avogadro: an advanced semantic chemical editor, visualization, and analysis platform, J. Cheminf. 4 (1) (2012) 17.
[35] M.T. Donor, S.A. Ewing, M.A. Zenaidee, W.A. Donald, J.S. Prell, Extended protein ions are formed by the chain ejection model in chemical supercharging electrospray ionization, Anal. Chem. 89 (9) (2017) 5107–5114.
[36] M.A. Zenaidee, M.G. Leeming, F. Zhang, T.T. Funston, W.A. Donald, Highly charged protein ions: the strongest organic acids to date, Angew. Chem. Int. Ed. 56 (29) (2017) 8522–8526.
[37] E.D.B. Foley, M.A. Zenaidee, R.F. Tabor, J. Ho, J.E. Beves, W.A. Donald, On the mechanism of protein supercharging in electrospray ionisation mass spectrometry: effects on charging of additives with short- and long-chain alkyl constituents with carbonate and sulphite terminal groups, Anal. Chim. Acta 1 (2019) 100004.
[38] M.A. Zenaidee, W.A. Donald, Extremely supercharged proteins in mass spectrometry: profiling the pH of electrospray generated droplets, narrowing charge state distributions, and increasing ion fragmentation, Analyst 140 (6) (2015) 1894–1905.
[39] C.A. Teo, W.A. Donald, Solution additives for supercharging proteins beyond the theoretical maximum proton-transfer limit in electrospray ionization mass spectrometry, Anal. Chem. 86 (9) (2014) 4455–4462.
[40] A.T. Iavarone, J.C. Jurchen, E.R. Williams, Supercharged protein and peptide ions formed by electrospray ionization, Anal. Chem. 73 (7) (2001) 1455–1460.
[41] A.T. Iavarone, E.R. Williams, Mechanism of charging and supercharging molecules in electrospray ionization, J. Am. Chem. Soc. 125 (8) (2003) 2319–2327.
[42] M.A. Zenaidee, Charging and Dissociation of Peptides and Intact Proteins Formed by Electrospray Ionisation, Ph.D. Thesis, University of New South Wales, Sydney, 2018.
[43] A.A. Shvartsburg, R.D. Smith, Ultrahigh-resolution differential ion mobility spectrometry using extended separation times, Anal. Chem. 83 (1) (2011) 23–29.
[44] E.V. Krylov, E.G. Nazarov, Electric field dependence of the ion mobility, Int. J. Mass Spectrom. 285 (3) (2009) 149–156.
[45] W.A. Donald, R.D. Leib, M. Demireva, E.R. Williams, Ions in size-selected aqueous nanodrops: sequential water molecule binding energies and effects of water on ion fluorescence, J. Am. Chem. Soc. 133 (46) (2011) 18940–18949.
[46] W.A. Donald, E.R. Williams, Evaluation of different implementations of the thomson liquid drop Model: comparison to monovalent and divalent cluster ion experimental data, J. Phys. Chem. A. 112 (16) (2008) 3515–3522.
[47] S. Zhu, J.L. Campbell, I. Chernushevich, J.C.Y. Le Blanc, D.J. Wilson, Differential mobility spectrometry-hydrogen deuterium exchange (DMS-HDX) as a probe of protein conformation in solution, J. Am. Soc. Mass Spectrom. 27 (6) (2016) 991–999.
[48] E.W. Robinson, E.R. Williams, Multidimensional separations of ubiquitin conformers in the gas phase: relating ion cross sections to H/D exchange measurements, J. Am. Soc. Mass Spectrom. 16 (9) (2005) 1427–1437.
[49] V.H. Wysocki, G. Tsaprailis, L.L. Smith, L.A. Breci, Mobile and localized protons: a framework for understanding peptide dissociation, J. Mass Spectrom. 35 (12) (2000) 1399–1406.
[50] J.S. Brodbelt, L.J. Morrison, I. Santos, Ultraviolet photodissociation mass spectrometry for analysis of biological molecules, Chem. Rev. 120 (7) (2020) 3328–3380.
[51] L.J. Morrison, J.S. Brodbelt, Charge site assignment in native proteins by ultraviolet photodissociation (UVPD) mass spectrometry, Analyst 141 (1) (2016) 166–176.
[52] A. Theisen, R. Black, D. Corinti, J.M. Brown, B. Bellina, P.E. Barran, Initial protein unfolding events in ubiquitin, cytochrome c and myoglobin are revealed with the use of 213 nm UVPD coupled to IM-MS, J. Am. Soc. Mass Spectrom. 30 (1) (2019) 24–33.
[53] A.A. Shvartsburg, A. Haris, R. Andrzejewski, A. Entwistle, R. Giles, Differential ion mobility separations in the low-pressure regime, Anal. Chem. 90 (1) (2018) 936–943.
[54] A.A. Shvartsburg, R. Andrzejewski, A. Entwistle, R. Giles, Ion mobility spectrometry of macromolecules with dipole alignment switchable by varying the gas pressure, Anal. Chem. 91 (13) (2019) 8176–8183.